Cell Biol Toxicol (2025) 41:65
https://doi.org/10.1007/s10565-025-10014-w

RESEARCH

Early endolysosomal dysfunction is a contributing factor to gadolinium-based contrast agent mouse renal proximal tubule epithelial cell injury

Joshua DeAguero · Tamara Howard · G. Patricia Escobar · Karol Dokladny · Brent Wagner

Received: 22 October 2024 / Accepted: 25 March 2025

Abstract The prevalence of contrast-enhanced magnetic resonance imaging (MRI) examinations and the absence of safer alternatives to gadolinium-based contrast agents (GBCAs) make the associated adverse effects of GBCAs much more concerning. Safety concerns arise from the toxic behavior of heavy metal gadolinium (Gd^{3+}) and the potential release of the metal from the chelating ligand. Renal insufficiency and other patient factors increase the susceptibility to the toxic effects of GBCAs. It is, therefore, imperative that the molecular and cellular mechanisms underlying GBCA toxicity be defined. This study aims to determine GBCA-induced endolysosomal dysfunction in mouse renal proximal tubule epithelial cells. Loss of cell viability was agent- and time-dependent, and proximal tubule injury was detectable following 24 h linear GBCA exposure. Both classes of GBCAs displayed lysosomotropic behaviors, characterized by early lysosomal enlargement and lysosomal injury. Hijacking of the endolysosomal system by these agents inhibited cathepsin processing by blocking the transport and maturation of cathepsin B (CTSB) and cathepsin D (CTSD). Lysosomal enlargement coincided with the translocation of CTSB and CTSD from the lysosomal lumen to the cytosol, suggesting lysosomal membrane destabilization. Even though both agents displayed a similar response, linear exposures appeared to exhibit a greater effect. Disturbance of mitochondrial activity and loss of cell viability occurs downstream of early lysosome damage. This effect was partially restored by lysosomal protease inhibitor co-treatment. This data suggests that GBCA exposures induce a lysosomal stress response, and partial LMP occurs upstream of mitochondrial dysfunction and resultant cellular injury.

Supplementary Information The online version contains supplementary material available at https://doi.org/10.1007/s10565-025-10014-w.

J. DeAguero (✉) · G. P. Escobar · K. Dokladny · B. Wagner (✉)
Kidney Institute of New Mexico, University of New Mexico Health Sciences Center, Albuquerque, NM, USA
e-mail: joshdeaguero@salud.unm.edu

B. Wagner
e-mail: brwagner@salud.unm.edu

G. P. Escobar
e-mail: gpescobar@salud.unm.edu

K. Dokladny
e-mail: kdokladny@salud.unm.edu

T. Howard
Department of Cell Biology & Physiology, University of New Mexico Health Sciences Center, Albuquerque, NM, USA
e-mail: thoward@salud.unm.edu

B. Wagner
New Mexico Veterans Administration Health Care System, Research Service, Albuquerque, NM, USA

Published online: 03 April 2025

Keywords Gadolinium-based contrast agents · MRI contrast · Renal tubular cell injury · Lysosomal damage · Cathepsins · Mitochondrial dysfunction

Introduction

Modern magnetic resonance imaging (MRI) contrast agents have undergone numerous iterations since they were first introduced for clinical use over 30 years ago (Lohrke et al. 2016). The commonality amongst these agents is the utilization of gadolinium (Gd^{3+}), a heavy metal in the lanthanide series, owing to its remarkable paramagnetic properties (Hermann et al. 2008). Despite its inherent clinical utility, Gd^{3+} is highly toxic and must be chelated with organic ligands to reduce its toxicity and promote *intact* renal elimination of the agent while retaining functionality (Wahsner et al. 2019). Gadolinium-based contrast-enhanced MRIs (CE-MRI) have been crucial in diagnosing various cancers and neurological diseases, cardiovascular diseases, arthritis progression, inflammatory bowel diseases, and numerous others (Lohrke et al. 2016). Generally considered safe for use, there are concerns over the potential toxicity of these agents to multiple tissues and organs owing to the direct insult of gadolinium (Sherry et al. 2009). Early adverse effects of these agents were first recognized in patients with renal insufficiency, which manifests as multiorgan fibrosis, clinically referred to as nephrogenic systemic fibrosis (NSF) (Shamam et al. 2024). The onset of NSF in these patients was directly associated with previous gadolinium exposures and thus began the journey of defining the mechanisms of toxicity.

Gadolinium-based contrast agents (GBCAs) are categorized into two general classes, linear or macrocyclic, although each agent has unique physicochemical properties (Do et al. 2021). Chemical structure, thermodynamic stability, charge, or the addition of excess chelate are purported to play a role in the mechanism of action of GBCA toxicity (Davies et al. 2022). The association of Gd^{3+}, or lack thereof, with its chelate has been attributed to the injuriousness of the metal, as the sequestration of Gd^{3+}, regardless of renal function, in numerous tissues and vital organs has been well documented (Le Fur et al. 2023). Nonetheless, preclinical and clinical studies have established that Gd^{3+}, the agent itself, or a combination of the two exert a toxic effect (Davies et al. 2022). The mode of action of GBCAs and/ or Gd^{3+} on the molecular and cellular mechanisms of toxicity has yet to be fully expounded and is necessary to identify potential targets.

GBCAs are nephrotoxic as they are known to impair renal function, trigger cell death in proximal tubular cells, promote renal fibrosis, and impair renal metabolism (Heinrich et al. 2007; Do et al. 2019). However, how GBCAs exert this effect in the renal epithelium is widely unknown. Intracellular organelles, including mitochondria, endoplasmic reticulum, and lysosomes, play essential roles in maintaining cellular homeostasis in the kidney (Li et al. 2022). Lysosomes are membrane-bound acidic organelles that house an array of enzymes responsible for the degradation of macromolecules, damaged organelles, and other cellular material delivered via endocytosis, phagocytosis, or autophagy (Perera and Zoncu 2016). Still, recent advances in lysosomal biology highlight greater importance. The acidic organelle is now viewed as a highly dynamic signaling hub that aids cell homeostasis in coping with environmental stress (Lawrence and Zoncu 2019). Lysosomes are an integral part of the renal epithelial molecular machinery that facilitates normal renal physiology. Lysosomal dysfunction can disrupt autophagic flux, which manifests in mitochondrial dysfunction, promoting the progression of kidney disease (Li et al. 2022). Under increasingly stressful conditions, the lysosome can become destabilized, and cell fate depends on the degree of lysosomal membrane permeabilization (LMP). Complete lysosomal membrane rupture or partial LMP (pLMP) can occur, and the selective release of lysosomal content will initiate a cell signaling cascade, leading to cell injury and death (Patra et al. 2023).

Our previous study identified potential cellular targets of GBCAs. Repeated linear GBCA exposures in vivo impacted the renal epithelium's mitochondrial integrity and resulted in endosome enlargement, often containing biosynthesized gadolinium nanoparticles (DeAguero et al. 2023). However, the detailed sequence of events in GBCA-induced renal tubular injury must be clarified. For this reason, the following study focuses on the direct effect of linear and macrocyclic GBCA exposures on the endolysosomal system and how renal proximal tubule epithelial cells adapt to lysosomal stress, as GBCA properties (Table 1) can greatly influence toxic behavior.

Materials and methods

Cells and GBCA treatment

Mouse renal proximal tubular epithelial cells (MRPTEpiCs) (ScienCell Research Laboratories, #M4100-57) were cultured according to recommended protocols in complete epithelial cell medium-animal (c/EpiCM-a) (ScienCell Research Laboratories, #4131) and maintained at 37ºC and 5% CO_2. At 70% confluency, cells were washed 1 × with Dulbecco's phosphate buffered saline (DPBS) and treated with gadolinium-based MRI contrast agent Omniscan (Linear; GE Healthcare Inc., NDC 0407–0690-15) or Dotarem (Macrocyclic; Guebert LLC, NDC 67684–2000-3) at a physiologic concentration, 2 mM, using an estimated diagnostic dose (Friebe et al. 2018). Cells were incubated with either MRI contrast for 1 h, 4 h, 24 h, 48 h, or a 24 h GBCA exposure period *followed* by a 24 h washout period (cells washed 1 × with DPBS and incubated in GBCA-free medium for 24 h) and subsequently assayed or collected for further processing.

Lysosomal protease inhibitor treatment

To assess the role of lysosomal proteases in 24 h GBCA-exposed MRPTEpiCs, cells were incubated simultaneously with protease inhibitor cocktail (PI) (P1860, Sigma-Aldrich) at 1:400 dilution or cathepsin B inhibitor CA-074 methyl ester (CA-074Me) (S7420, SelleckChem) with the indicated contrast agents in c/EpiCM-a.

Quantification of intracellular gadolinium concentrations via inductively coupled plasma mass spectroscopy (ICP-MS)

To measure the amount of gadolinium in MRPTEpiCs as a measure of GBCA uptake, cells were seeded in a T75 flask at 10×10^3 cells/cm^2 and allowed to grow until 70% confluence. MRPTEpiCs were then incubated with either linear or macrocyclic GBCA for 1, 4, 24, and 48 h. Untreated cells at each time point served as controls. Following incubation, the media was removed, and the cells were washed once with DPBS, then harvested with trypsin, and centrifuged at 500 × *g* for 5 min. The media was aspirated, and the cell pellet was resuspended in c/EpiCM-a for cell counting. A final cell count of 1×10^6 for each sample was obtained. The cells were then pelleted by centrifugation at 500 × *g* and washed once with ice-cold 1X PBS. The pellet was washed 2 times with ultrapure distilled water to remove any residual isotonic buffer. The final water wash was aspirated, and the cells were resuspended in ultrapure distilled water to lyse osmotically. Samples were stored at −80° C until analysis. For ICP-MS analysis, the samples were diluted to 10 mL with 2% nitric acid for digestion. Gadolinium concentrations were quantified using PerkinElmer NexION 5000 inductively coupled plasma mass spectrometry with a detection limit of 0.01 ppb. The ICP-MS results are an average of triplicate experiments.

XTT cell viability assay

MRPTEpiCs were seeded at 10×10^3 cells/well in triplicate one day before GBCA exposure. The cells were incubated with linear or macrocyclic agents for 1 h, 4 h, or 24 h. Similarly, cells were co-incubated with lysosomal protease inhibitors for 24 h. To assess cellular metabolic activity as a measure of cell viability, the CyQuant™ XTT Cell Viability Assay (Thermo Fisher, #X12223) was used according to the manufacturer's protocol. Following the indicated treatment time points, the CyQuant™ XTT working solution was prepared, immediately added to the wells, and incubated according to the protocol. The XTT-specific absorbance was measured at 450 nm and 660 nm using the BioTek Synergy Neo2 Multi-Mode Reader (Agilent Technologies, Inc., USA).

Table 1 Properties of gadolinium-based contrast agents used in the study (Wahsner et al. 2019; Do et al. 2021)

Commercial Name	Chemical Name	Structure	Formal Charge	Agent Type	Formulation, % Excess Chelate
Omniscan	Gadodiamide	Linear	0	Non-specific extracellular	0.5 M, CA-DTPA-BMA 5%
Dotarem	Gadoterate meglumine	Macrocyclic	−1	Non-specific extracellular	0.5 M, 0%

LysoTracker red staining, imaging and analysis

MRPTEpiCs were seeded on sterile glass coverslips (15 mm round German glass, Bellco Glass, Inc., #1943-10015A) and treated as above. After indicated treatments and time points, cells were probed with 65 nM LysoTracker™ Red DND-99 (Thermo Fisher, # L7528) in EpiCM-a under optimal growth conditions (37 °C, 5% CO_2) for 1 h. Coverslips were then gently washed with warm PBS and fixed with 4% methanol-free formaldehyde. Following fixation, cells were counterstained with 4',6-diamidino-2-phenylindole (DAPI) and mounted with ProLong™ Glass Antifade Mountant (Thermo Fisher, #P36980). Images were captured shortly after using the Leica TCS-SP8 inverted confocal microscope (Leica Microsystems, Germany); random fields were selected, and images were obtained. For analysis, the DAPI channel was used to select cells to avoid user bias; the corresponding LTR images were analyzed for cellular fluorescence or quantitation of LTR-positive puncta. Cellular fluorescence was measured using FIJI/ImageJ (ImageJ 1.54f, NIH, USA), and data is represented as corrected total cellular fluorescence. Quantitative analysis of late endosome/ lysosome populations (LTR positive puncta) was performed using FIJI/ImageJ. The LTR channel was thresholded, cells selected in the DAPI channel were traced, and the Analyze Particles function was utilized; a range of LTR puncta sizes was established (0.1–5.0 μm^2) before analysis of all groups. A ratio of LTR-positive puncta numbers per cell area was established.

Immunofluorescence, imaging and analysis

Cells were seeded on 15 mm coverslips, as above, and allowed to reach 70% confluency before the indicated GBCA exposure. Following the designated time points, cells were fixed with 4% methanol-free paraformaldehyde for 15 min at 37ºC, then permeabilized with 0.1% Tween-20 in PBS for 10 min. Coverslips were blocked with 1% gelatin in KPBS for 10 min and washed accordingly. The cells were then singly stained or multiplexed overnight at 4ºC with the following primary antibodies: LAMP-1 (Thermo Fisher, #14–1071-85), Galectin-3 (Thermo Fisher, #PA5-7959), RAB7 (Thermo Fisher, #PA5-52369), cathepsin B (R&D Systems, #AF965), cathepsin D (R&D Systems, AF1029). After the overnight period, the coverslips were gently washed three times and subsequently incubated with corresponding secondary antibodies: Alexa Fluor 488-conjugated donkey anti-goat (Thermo Fisher, #A32814), Alexa Fluor 555-conjugated donkey anti-rabbit (Thermo Fisher, #A-31572), or Alexa Fluor 647-conjugated donkey anti-rat (Thermo Fisher, #A78947). Coverslips were then counterstained with DAPI to label the nuclei and mounted with ProLong™ Glass Antifade Mountant. Images were captured by the Leica TCS-SP8 confocal microscope using the sequential scanning function to avoid fluorophore crosstalk. Random visual fields were selected for imaging while maintaining the same setting parameters across experiments. Lysosomal size was quantified by measuring the diameter of LAMP-1-positive granules using FIJI/ImageJ. Briefly, cells were chosen in the DAPI channel to avoid user bias; the LAMP-1 channel was appropriately thresholded, and selected cells were traced. The Analyze Particles function was used to obtain the average diameter of LAMP-1-positive granules in each cell measured. To quantify endogenous punctate galectin-3 staining, at least 10 cells per random field were selected in the DAPI channel. The galectin-3 channel was thresholded, and the Analyze Particles highlighted cells displaying punctate galectin-3 (sizes of galectin-3 puncta pre-determined using positive control: 0.05–1.00 μm^2) and the percentage of cells scoring positive for galectin-3 dots was determined across all exposure groups.

Transmission electron microscopy

For conventional transmission electron microscopy, cells were grown in 100 mm cell culture dishes and treated at the appropriate confluence. MRPTEpiCs were collected and processed via the pellet method. After the indicated treatments, cells were washed once with DPBS and then trypsinized; trypsin was then inactivated with complete EpiCM-a. The suspension was centrifuged at $500 \times g$ for 5 min to pellet the cells. The pellet was then fixed in pre-warmed serum-free EpiCM-a containing 2% glutaraldehyde and 3% formaldehyde for 1 h at room temperature. Following fixation, the cells were centrifuged at $500 \times g$ for 10 min, and the pellet was subsequently washed three times with PBS. The pellets were then post-fixed with 1% tannic acid for 1 h at room temperature and washed three times with ultrapure

distilled water. Samples were then dehydrated in a stepwise series of ethanol exchanges for 10 min each: 20% > 40% > 60% > 80% > 100% (anhydrous) three times. The pellets were then exchanged to a 1:1 100% (anhydrous) ethanol: acetone mix for 10 min, followed by three acetone washes, centrifuging at $500 \times g$ between washes. The samples were then infiltrated with a 1:1 resin: acetone mix for 2 h. The resin mix was removed and replaced with 100% resin for an overnight infiltration. The following morning, the full resin was refreshed for 2 h, followed by a final resin change before polymerization in a 60 °C oven for at least 72 h. The samples were then trimmed and sectioned at 60–80 nm. The ultrathin sections were stained with uranyl acetate and lead citrate, and images were acquired using the Hitachi HT7700 transmission electron microscope with an AMT 16-megapixel camera (Hitachi, Ltd., Japan) operating at 80 kV. Random fields of view with ≥ 75 cells per group were obtained.

Multiplex fluorescent western blotting

Following the indicated treatments and time points, cells were lysed on ice in RIPA buffer (Thermo Fisher, #89901) containing Halt Protease Inhibitor cocktail without EDTA (Thermo Fisher, #87786). The BCA Protein Assay Kit (Thermo Fisher, #23225) was used to measure total protein concentrations. The samples were prepared in Laemmli sample buffer (Bio-Rad, #161–0747) with 2-mercaptoethanol (Bio-Rad, #161–0710) and boiled at 95 °C for 5 min. Prepared samples were run on Mino-PROTEAN® TGX™ 4–20% polyacrylamide gel (Bio-Rad, #456–1094) at 120 V for 90 min. The gels were subsequently transferred onto a 0.2 µm nitrocellulose membrane (Bio-Rad, # 1704158) using a Trans-Blot Turbo Transfer System (Bio-Rad). Membranes were blocked in 5% non-fat dry milk in TBST for 1 h at room temperature and then incubated overnight at 4 °C with primary antibodies: KIM-1 (R&D Systems, #AF1817) or cathepsin B (R&D Systems, # AF965) or cathepsin D (Proteintech, #21327–1-AP), and β-actin (Proteintech, #66009–1-Ig). After overnight incubation, the membranes were washed 3 times with TBST and then incubated with corresponding fluorescent secondary antibodies for 90 min at room temperature: IRDye® 800CW donkey anti-goat (LI-COR Biotech, 926–32214), IRDye® 800CW donkey anti-rabbit (LI-COR Bitoech, 926–32213), IRDye® 680LT donkey anti-mouse (LI-COR Biotech, 926–68022). Membranes were imaged on an Odyssey® DLx infrared imaging system (LI-COR Biotech LLC, USA). Signal intensities for the respective bands were obtained using the companion software Image Studio™ (version 5.5.4, LI-COR Biotech). The signals were normalized to internal loading control β-actin, and a normalization factor was obtained for each lane/blot, resulting in a normalized experimental signal. Data from at least three independent experiments are expressed as relative protein quantities in GBCA-exposed MRPTEpiCs to that of the corresponding protein in untreated cells.

Measurement of cathepsin B activity

To assess cathepsin B activity after 4 and 24 h exposure, cells were seeded at 10×10^3 cells/cm^2 in 100 mm cell culture dishes and treated at the appropriate confluence. According to the manufacturer's protocol, activity was measured using a fluorescence-based assay (Abcam, #ab65300). Following the appropriate incubation conditions, cells were harvested and lysed with the kit's Cathepsin B Cell Lysis Buffer. Protein concentrations were obtained for each sample using the BCA Protein Assay Kit and 50 µg of protein was used for each reaction well, in replicate. The appropriate volumes of reaction buffer and Cathepsin B substrate were added to the reaction wells and incubated according to the protocol. The released AFC (amino-4-trifluoromethyl coumarin) was measured at 400 nm and 505 nm using the BioTek Synergy Neo2 Multi-Mode Reader (Agilent Technologies, Inc., USA).

MitoTracker Red-FM live cell imaging and mitochondrial network analysis

Following the indicated time points and treatments, MRPTEpiCs were stained with the MitoTracker Red-FM probe (Thermo Fisher, #M22425) at a concentration of 250 nM in serum-free EpiCM-a for 30 min under appropriate growth conditions (37 °C, 5% CO_2). The staining solution was then removed and replaced with fresh pre-warmed EpiCM-a. Shortly after, live-cell imaging was performed using the Leica TCS-SP8 confocal microscope. Random fields of view were swiftly obtained for each treatment

group, maintaining the same setting parameters across all experiments. For analysis purposes, single-cell mitochondrial network structure was quantified using the FIJI/ImageJ Mitochondria Analyzer plugin (Chaudhry et al. 2020). The 2D Threshold Optimize command defined the optimal thresholding settings before advancing through the 2D pipeline. The images were thresholded (2D Threshold) following this optimization step with the default settings applied, albeit with the following adjustments: the 'Enhance Local Contrast' was deselected, and a Block Size of 1.35 and C-Value of 5 was used. 2D analysis was performed per cell, and the output of mitochondrial morphological descriptors was compared between time and treatment groups.

Measurement of mitochondrial membrane potential

To measure mitochondrial membrane potential ($\Delta\Psi m$), the TMRE Mitochondrial Membrane Potential Assay Kit (Cayman Chemical, #701310), which utilizes fluorescent dye tetramethylrhodamine ethyl ester (TMRE), was used according to the assay protocol. MRPTEpiCs were seeded in black 96-well clear bottom plates and allowed to reach 70% confluence before treatment. Following the time points and treatments, each experimental well was probed with 25 nM TMRE for 30 min at 37 °C, 5% CO_2. Once stained, the wells were washed twice with the assay buffer, and fresh buffer was added to each well. The plate was equilibrated at room temperature for 20 min before reading at an excitation of 530 nm, and emission of 580 nm, using the fluorescence function of the Neo2 multi-mode plate reader (Agilent Technologies, Inc., USA). A relative fluorescence signal was obtained for each group from at least three independent experiments.

Statistical analysis

RStudio (2023.06.01 + 5244 "Mountain Hydrangea") was used for statistical analyses and graph plotting. Statistical comparisons were made using one-way or two-way analysis of variance (ANOVA) with post-hoc Tukey HSD (Honestly Significant Difference). A p-value less than 0.05 was considered statistically significant, and the p for statistically significant data is numerically denoted in the appropriate graphs, or ns = not significant.

Results

Gadolinium accumulates intracellularly in response to GBCA exposure

To analyze the agent- and time-dependent accumulation of gadolinium, a surrogate measurand for GBCA cellular uptake, MRPTEpiCs were treated with a physiological concentration of 2 mM (using estimated diagnostic dose) (Friebe et al. 2018) for 1, 4, 24, and 48 h of either linear or macrocyclic GBCA (Fig. 1a). Overall bulk analysis of gadolinium concentrations by ICP-MS between untreated and GBCA treated groups displayed remarkable differences in gadolinium levels, as gadolinium is a non-physiological element. As early as 1 h of exposure to either class of GBCA, gadolinium levels were significantly increased, suggesting early GBCA uptake. Analysis of each time point, up to 48 h exposure, confirms gadolinium accumulation, indicating the intracellular uptake of GBCAs (Fig. 1b). This cellular association of gadolinium suggests a rate of uptake that increases in parallel with the incubation periods, irrespective of GBCA class. This data speaks in favor of intracellular uptake of the extracellularly designed agents.

GBCAs are injurious to renal proximal tubules in a time-dependent manner

For the remainder of the study, we focused on time points up to 24 h GBCA exposure. An XTT colorimetric assay was used to monitor the metabolic activity of GBCA-treated cells and indicate cell viability. The conversion of the yellow tetrazolium salt to an orange-colored formazan product was used to quantify metabolically active cells (Fig. 2a). The 1 and 4 h time points showed no significant changes in the activity of the GBCA-treated cells. However, 24-h exposure to linear GBCAs resulted in a reduced metabolic capacity. To further determine whether these agents were injurious to MRPTEpiCs, kidney injury molecule-1 (KIM-1), a biomarker of drug-induced nephrotoxicity, was used to monitor proximal tubule injury. Expression of KIM-1 in normal renal tubular cells is low, but upon insult, overexpression of KIM-1 correlates with the extent of kidney damage, making it a valuable biomarker for toxicity (Song et al. 2019). After 24-h linear GBCA treatment, protein levels of KIM-1 increased compared to untreated

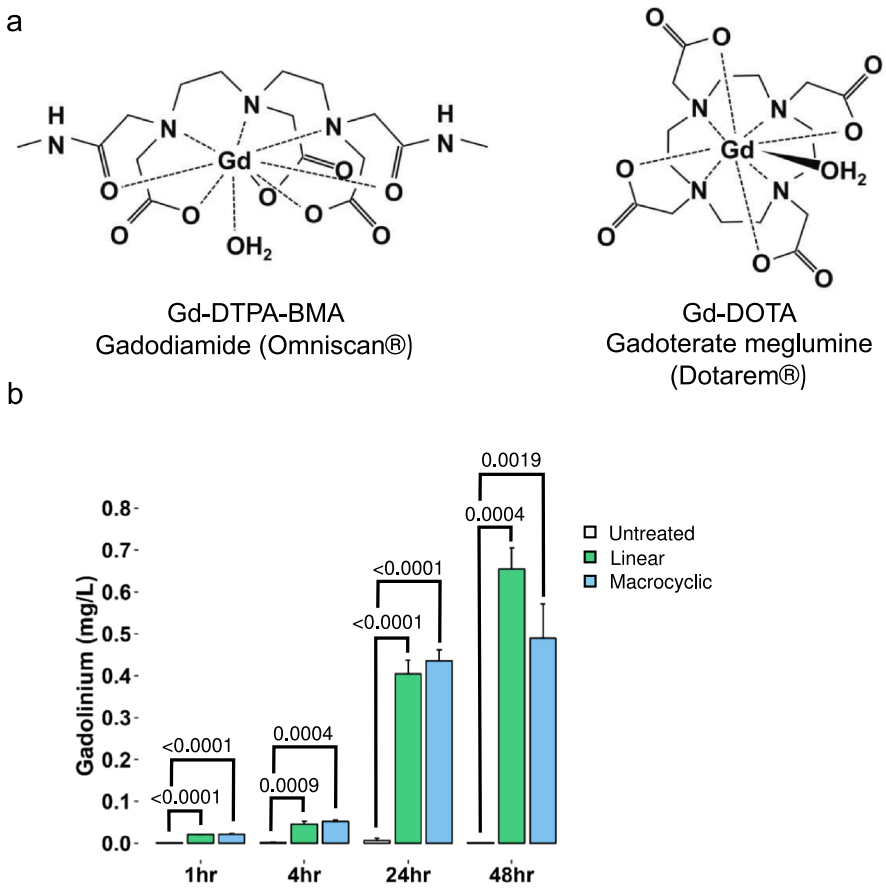

Fig. 1 Intracellular accumulation of linear and macrocyclic gadolinium-based contrast agents. **a**. Chemical structures, chemical names, and generic and brand names of the linear and macrocyclic gadolinium-based contrast agents used in this study. **b**. Gadolinium concentrations in MRPTEpiCs at 1, 4, 24, and 48 h GBCA exposure, as assayed by ICP-MS. Gadolinium levels were obtained from 1×10^6 cells, with each value representing the mean of triplicate experiments ± SEM ($n = 3$ per group). The p-values are denoted numerically, from Untreated, by One-way ANOVA, Tukey honesty significant difference post-hoc testing

controls; treatment with macrocyclic GBCA showed no increase in protein expression of the biomarker (Fig. 2b). These data indicate that linear GBCAs are injurious to renal proximal tubule epithelial cells in a time-dependent manner.

Linear contrast agent treatment, in vivo, results in distinct morphological changes of tubular injury characterized by vacuolization, accumulation of unilamellar vesicles, profound mitochondrial injury, and the biosynthesis of gadolinium nanoparticles (DeAguero et al. 2023). Additionally, in vivo, treatment with macrocyclic contrast agents resulted in similar morphological changes, including alterations to mitochondrial ultrastructure (Supplementary Fig. S1a, upper) and enlarged endosomes with lipid and electron-dense cargo (Supplementary Fig. S1a, middle). These morphological changes are further characterized by the intracellular accumulation of unilamellar vesicles (Supplementary Fig. S1a, lower). In addition, treatment of either class of GBCAs resulted in the development of concentric structures referred to as lamellar bodies (Supplementary Fig. S1b), a hallmark of phospholipidosis. This in vivo data suggests that critical organelles, particularly the mitochondria and endolysosomes, are either the initiator or target of GBCAs. Lysosomotropic dye, LysoTracker Red DND-99 (LTR), accumulates in intact lysosomes and other acidic cellular compartments by acidotropsim and was used to monitor the integrity of the endolysosomal system in this exposure model. LTR cellular fluorescence was evaluated following 1, 4, and 24 h exposures to either agent (Fig. 2c). A 1 h exposure to the linear GBCA resulted in a nominal decrease in LTR staining, with a slight LTR fluorescence increase in the macrocyclic group (Fig. 2c). After 4 h exposures to both agents, there was a marked decrease in LTR staining compared to untreated controls, whereas after 24 h exposure to either agent resulted in a highly pronounced LTR fluorescence as seen in Fig. 2d. The decrease in LTR fluorescence at 4 h suggests alterations to lysosomal integrity. To address the drastic increase in LTR fluorescence after 24 h

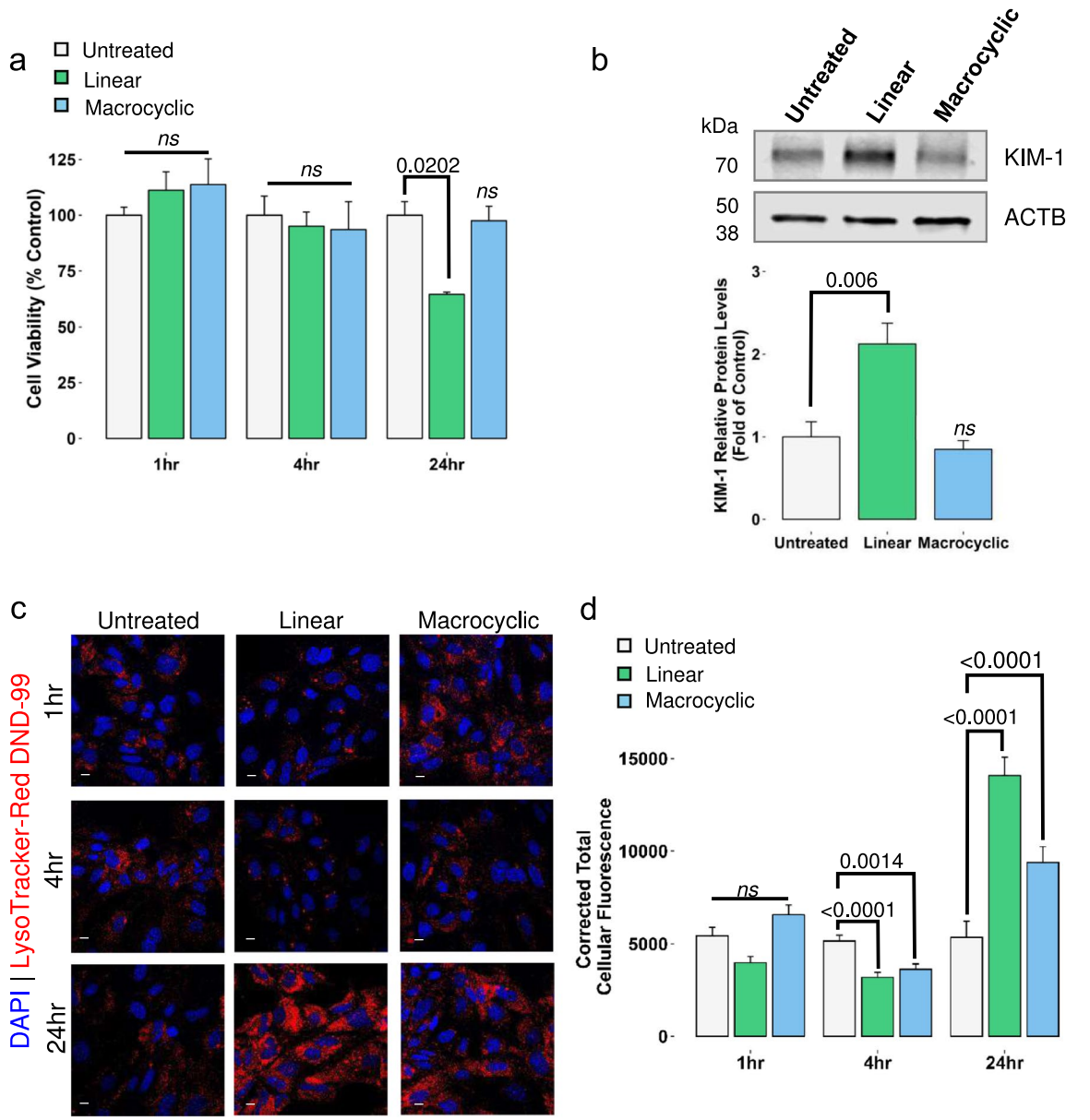

Fig. 2 Time- and agent-dependent effects of GBCA exposures on MRPTEpiC function. **a**. Impact of 1 h, 4 h, and 24 h GBCA exposures on cell viability using the XTT assay. Cell viability is expressed as the percentage of metabolically active cells after the indicated GBCA exposures. Results are represented as mean ± SEM ($n = 3$ per group). The p-values are denoted numerically, ns = not significant from Untreated, by One-way ANOVA, Tukey honesty significant difference post-hoc testing. **b**. Quantitative western blot analysis of relative kidney injury molecule-1 (KIM-1) following 24 h GBCA exposures. Data are represented as mean ± SEM ($n = 4$). **c**. Representative confocal images of LysoTracker Red-DND-99 (LTR) probing at 1 h, 4 h, and 24 h GBCA exposure. Cell loaded with 65 nM LTR and nuclei counterstained with 4',6-diamidino-2-phenylindole (DAPI). Leica TCS SP8. Bars = 10 µm. **d**. Quantification of the corrected total cellular fluorescence of LTR compared to untreated at the respective time points. Results are represented as mean ± SEM from ≥ 65 cells ($n = 3$). The p-values are denoted numerically, ns = not significant from Untreated, by One-way ANOVA, Tukey honesty significant difference post-hoc testing

exposure, populations of LTR-positive puncta were quantified. Increases in LTR staining could indicate changes in endolysosomal volume, as lysosomal biogenesis is often a compensatory mechanism for cell survival in response to lysosomal insult (Papadopoulos et al. 2020). LTR-positive puncta population density increased at least twofold in both exposure groups at 24 h compared to untreated controls (Supplementary Fig. S2). In addition, to address whether this increase in LTR-positive puncta populations is a transient response to the 24-h GBCA exposure, an additional series of experiments was conducted. Following the established 24 h exposure model, cells were afforded a 24 h washout period. Linear exposure with washout (Linear-WO) treated cells sustained the increase in LTR puncta compared to the untreated washout control, albeit reduced to linear alone (Supplementary Fig. S2b). Macrocyclic exposure with washout (Macrocyclic-WO) maintained a similar trend but to a lesser extent than the linear groups, as shown in Supplementary Fig. 2. Thus far, these data suggest not only that linear GBCAs are injurious to renal proximal tubule epithelia but also that GBCAs alter lysosomal functionality.

Exposure to GBCAs induce endolysosomal enlargement

Functional lysosomes are essential to maintaining cellular homeostasis. Dysfunctional lysosomes are involved in various diseases, including lysosomal storage diseases, neurodegeneration, and cancer (Cao et al. 2021). Changes in the expression or activity of lysosomal enzymes, alterations in the size, number, and position of lysosomes, and destabilization of the lysosomal membrane are critical features of lysosomal dysfunction (Wang et al. 2018a, b). Innumerable external and internal stimuli, including lysosomotropic agents, can lead to this dysfunction. Because of the apparent changes to the endolysosomal system, as observed by changes in LTR staining patterns seen in Fig. 2, it was pertinent to understand the effect of GBCAs on lysosome and lysosomal-related organelle structure. Lysosomal-associated membrane protein 1 (LAMP-1), a well-characterized lysosomal membrane protein, was used as a marker of lysosomes in this exposure model (Fig. 3a). To monitor changes in LAMP-1 positive lysosomes at 4 h and 24 h post-exposure, we quantitively analyzed the size of these organelles. A 4 h exposure period increased the diameter of LAMP-1 lysosomes in both GBCA groups compared to the untreated control (Fig. 3b, left). Lysosomes in the 24 h exposure groups are further characterized by a continual enlargement of LAMP-1 organelles, as seen in Fig. 3b, albeit with linear exposed lysosomes being characteristically larger. At this point, the data confirms GBCA exposure leads to enlargement of the lysosome, but whether this enlargement is detrimental to the lysosomes remains unclear.

Intracellular galectins are well-studied as markers of endolysosomal damage. They form distinct puncta as part of the multi-tiered response to endomembrane damage (Aits et al. 2015a, b). Galectin-3 (Gal-3) functions during lysosomal damage and was used as a damage marker in this study, as changes from a diffuse cytoplasmic staining pattern to distinct puncta are observable by confocal microscopy (Fig. 3c). LAMP-1 was again used as a lysosomal marker to determine the proximity of Gal-3 staining. The percentage of cells expressing endogenous, cytoplasmic Gal-3 puncta was quantified. Cells positive for Gal-3 puncta staining were observable at 4 h and 24 h exposure, regardless of the agent (Fig. 3d). Interestingly, more Gal-3 positive cells were detected at the 4 h exposure time point compared to 24 h exposure. This suggests that not only does 4 h GBCA exposure induce lysosomal enlargement, but it also prompts lysosomal injury. Furthermore, the decrease in Gal-3 positive cells at 24 h may indicate lysosomal repair and removal. We used TEM to observe these morphological changes to further visualize the abnormal enlargement of LAMP-1 lysosomes at 4 and 24 h exposure. As early as 4 h exposure, in conjunction with the confocal microscopy data, cell exposed to either class of GBCA displayed the aggregation of numerous enlarged vesicles (Fig. 3e, upper). Cells exposed to either agent for 24 h exhibited swelling of organelles and profound formation of vacuoles (Fig. 3e, lower). Linear exposed cells displayed a more drastic response and signs of nuclear fragmentation, indicating GBCA-induced cell death. In addition, at the 24-h time point, cells were co-stained for markers of the endolysosomal system: late endosome marker RAB-7 and lysosomal marker LAMP-1. Consistent with the TEM studies, confocal microscopy further highlights that GBCA exposure in kidney cells affects the endolysosomal system and the development of enlarged endolysosomal structures

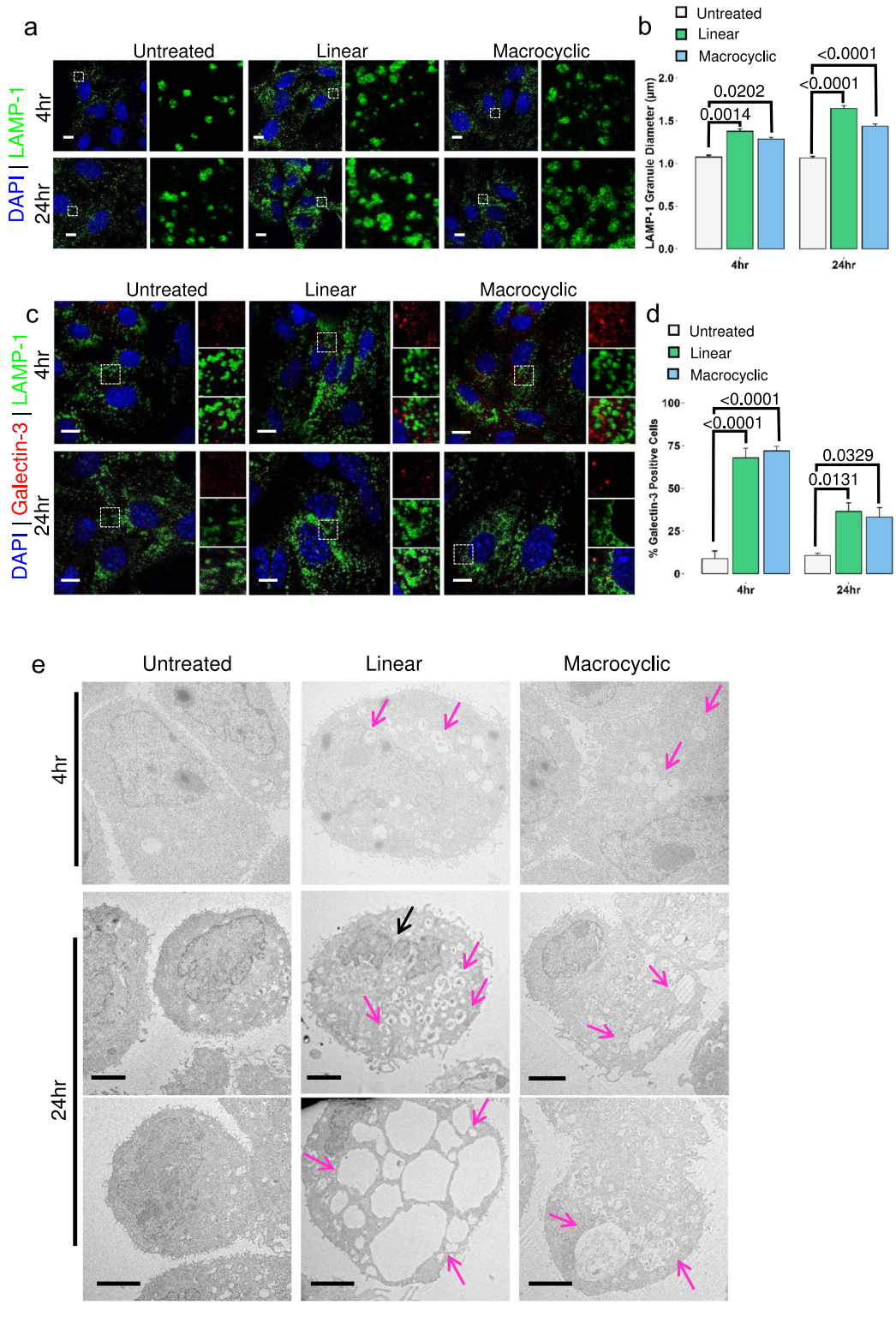
a
Untreated
Linear
Macrocyclic
DAPI | LAMP-1
4hr
24hr
b
Untreated
Linear
Macrocyclic
LAMP-1 Granule Diameter (μm)
0.0202
0.0014
<0.0001
<0.0001
4hr
24hr
c
Untreated
Linear
Macrocyclic
DAPI | Galectin-3 | LAMP-1
4hr
24hr
d
Untreated
Linear
Macrocyclic
% Galectin-3 Positive Cells
<0.0001
<0.0001
0.0329
0.0131
4hr
24hr
e
Untreated
Linear
Macrocyclic
4hr
24hr

◂**Fig. 3** GBCA-induced lysosomal enlargement and injury. **a**. Lysosomal-associated membrane protein 1 (LAMP-1) (green) expression and distribution in untreated and GBCA exposed cells. Nuclei counterstained with DAPI. Higher magnification of the region of interest is denoted by the dashed box and displayed adjacent to the respective image. Leica TCS SP8. Bars = 10 µm **b**. Quantification of LAMP-1 granule diameter in untreated and treated cells following 4 h and 24 h exposures. Results are represented as mean ± SEM from ≥ 50 cells ($n = 3$). The *p*-values are denoted numerically and determined by Two-way ANOVA, Tukey honesty significant difference post-hoc testing. **c**. Representative images of galectin-3 translocation assay in GBCA-exposed MRPTEpiCs at the indicated time points. Higher magnification of the merged region of interest is denoted by the dashed box and displayed adjacent to the respective image: Galectin-3 (Upper), LAMP-1 (Middle), Merge (Lower). Leica TCS SP8. Bars = 10 µm. **d**. Quantification of galectin-3 positive cells in untreated and treated MRPTEpiCs at 4 h and 24 h GBCA exposure. Results are represented as mean ± SEM from ≥ 75 cells ($n = 3$). The *p*-values are denoted numerically and determined by Two-way ANOVA, Tukey honesty significant difference post-hoc testing. **e**. Transmission electron microscopy images of MRPTEpiCs following 4 and 24 h exposure highlighting vacuolization (magenta arrows). Nuclear fragmentation (black arrow). $n \geq 75$ cells per group. Hitachi HT7000 TEM, AMT 16-megapixel digital camera. Bars = 2.5 µm

(EELs) (Supplementary Fig. S3). These results, taken together, suggest that 4 h exposure to either linear or macrocyclic is the initiating time point at which lysosomal injury and enlargement of LAMP-1-positive lysosomes are present.

GBCAs induce lysosomal dysfunction and partial lysosomal membrane permeabilization

To investigate how GBCAs might alter lysosomal function and whether GBCA-induced lysosomal enlargement is a pre-requisite for lysosomal membrane destabilization, we monitored the expression and localization of cysteine protease cathepsin B (CTSB) and aspartic protease cathepsin D (CTSD) in response to GBCA exposure. CTSB and CTSD are the most abundant lysosomal proteases and play critical cellular functions, including late-stage roles in autophagy (Yadati et al. 2020). The cellular outcome of lysosomal stress often depends upon the extent of LMP influenced by the size of the pores formed in the lysosomal membrane. The degree of LMP will dictate the selective translocation of lysosomal content into the cytoplasm and the compensatory mechanisms initiated by the cell (Wang et al. 2018a, b). To examine how GBCA exposure and potential LMP affect the processing of CTSB, intracellular levels of the protein were assessed by western blot at 4 h (Fig. 4a) and 24 h (Fig. 4d) exposure. ProCTSB autoproteolytically activates itself into mCTSB within endo/lysosomes (Turk et al. 2001). Exposure to both linear and macrocyclic agents for 4 h significantly impaired the maturation of CTSB (mCTSB) (Fig. 4c). GBCA exposure at either time point produced no significant changes to proCTSB levels. However, mCTSB protein levels were restored to a certain degree when compared to untreated levels following 24 h exposure to both agents (Fig. 4f). Our data show that a 4 h exposure to either type of agent results in early lysosomal dysfunction.

To further determine whether LMP occurs in GBCA-exposed cells, cathepsin localization was monitored by confocal microscopy as lysosomal proteases will translocate from the lysosomal lumen to the cytosol in response to LMP. Immunostaining data from the untreated controls showed a consistent colocalization of CTSB with LAMP-1 at both the 4 h and 24-h time points (Fig. 4g, left), indicating that the LAMP-1 positive lysosomes in this cell type are positive for lysosomal proteases and that these organelles have a degradative capacity. A bright, diffuse staining pattern was observed at both the 4 h and 24 h time points in linear GBCA exposed cells (Fig. 4g, middle), indicating a degree of LMP. Macrocyclic exposed cells displayed a brighter punctate staining pattern with increased cytoplasmic diffusion at 24 h compared to 4 h (Fig. 4g, right), suggesting a time-dependent release of CTSB.

CTSD is trafficked as a pro-form via the endocytic pathway to the lysosome, where it undergoes proteolysis-mediated maturation to mCTSD by CTSB and cathepsin L. Intracellular protein levels of CTSD were also assessed by western blotting at 4 h (Fig. 5a) and 24 h (Fig. 5d). Quantitative analysis revealed that levels of proCTSD decreased in both linear and macrocyclic exposed cells at 4 h compared to untreated protein levels (Fig. 5b). At the same time, mCTSD levels in linear 4 h-exposed cells showed a similar response (Fig. 5c). Macrocyclic exposure displayed a similar response but to a lesser degree. At the 24-h time point, proCTSD and mCTSD returned to near untreated levels, as seen in Fig. 5e-f. At 4 h exposure, levels of pro-forms of CTSD were significantly altered in both linear and macrocyclic GBCA-exposed groups. In contrast, only linear exposure for 4 h significantly reduced mCTSD protein levels,

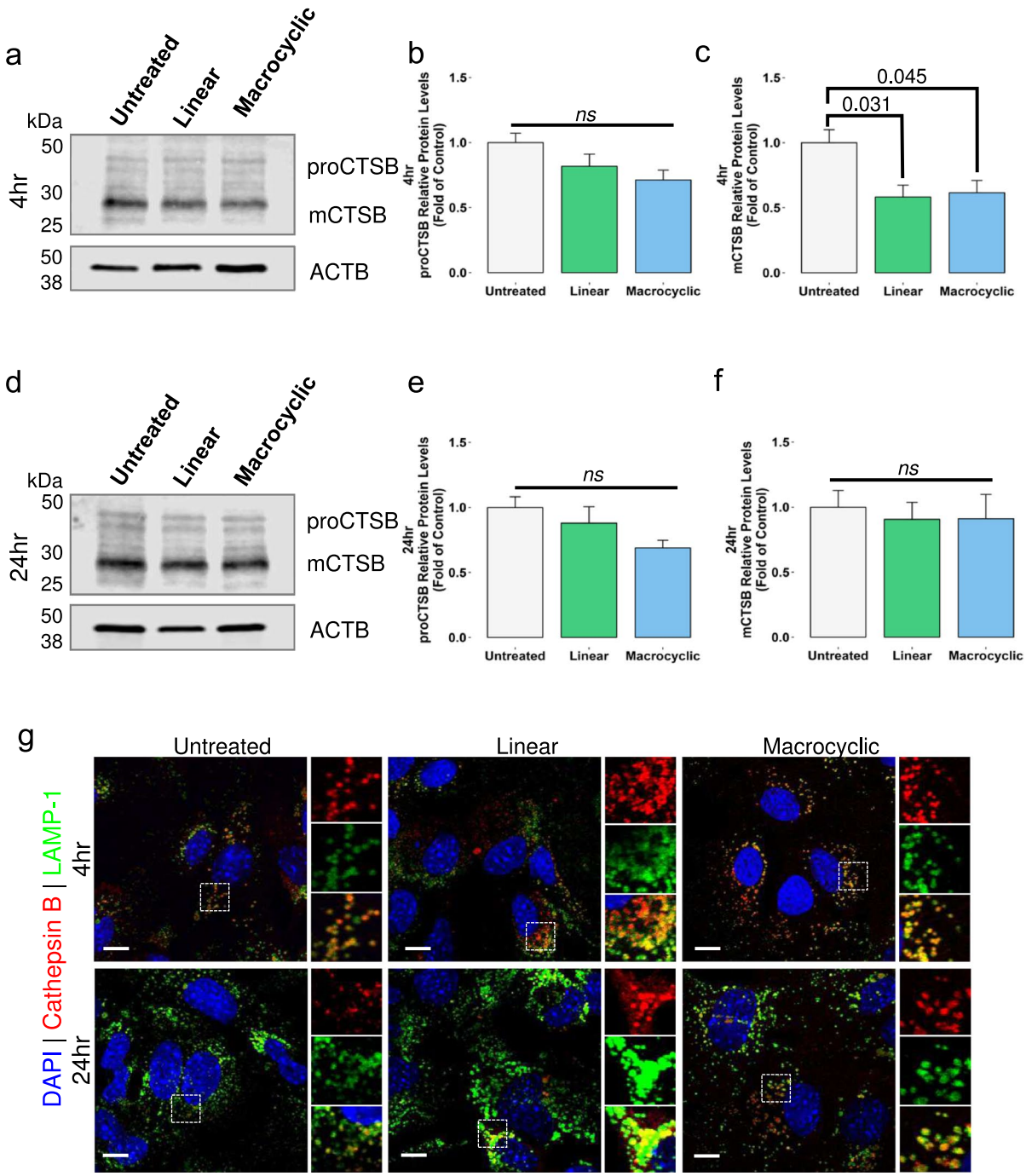

Fig. 4 Effect of GBCAs on cathepsin B processing and lysosomal membrane permeabilization. **a**. Representative western blot showing levels of CTSB in MRPTEpiCs following 4 h exposure. **b-c**. Quantitative analysis of relative proCTSB and mCTSB levels in untreated and exposed groups, respectively. **d**. Western blot displaying the expression levels of CTSB after 24 h linear or macrocyclic GBCA exposure. **e–f**. Quantification of relative protein levels of proCTSB and mCTSB following exposure. **b-c-e–f.** Data represented as mean ± SEM ($n = 4$ per group). The p-values are denoted numerically, *ns* = not significant from Untreated, by One-way ANOVA, Tukey honesty significant difference post-hoc testing. **g**. Representative confocal images of CTSB and LAMP-1 staining patterns in GBCA-exposed MRPTEpiCs from at least three independent experiments. Inset dashed boxes indicate regions of interest highlighted by magnified adjacent images: CTSB (Upper), LAMP-1 (Middle), and Merge (Lower). Nuclei were counterstained with DAPI. Leica TCS SP8. Bars = 10 µm

indicating altered cathepsin processing. This response indicates potential linear-induced degradation of CTSD or less transport of proCTSD to the lysosome, resulting in reduced formation of mCTSD or reduced proteolysis of proCTSD into mCTSD by CTSB. Given the dynamic role of cathepsin B in the turnover of proteins, particularly the maturation of cathepsin D, it was important to assess the activity of CTSB at 4 and 24 h exposure. A 4 h GBCA exposure resulted in a non-significant increase in CTSB activity (Supplementary Fig. S4a). Further exposure to either agent proceeded to significantly increase CTSB activity at 24 h exposure (Supplementary Fig. S4b). These data suggest the effect of GBCA exposure on CTSD protein expression levels is multifactorial. Reduced levels of proCTSD at 4 h and near-normal CTSB activity suggest reduced endocytic trafficking of the pro-peptide to the lysosome. Additionally, GBCA-induced low levels of mCTSB at 4 h further indicate reduced processing of proCTSD into mCTSD, highlighting reduced lysosomal stability at 4 h exposure, leading to dysfunctional lysosomes. Altogether these data indicate that the intracellular accumulation of GBCAs leads to the dysregulation of cathepsins.

Like CTSB in untreated controls, immunofluorescence of CTSD shows confinement to LAMP-1-positive lysosomes at both time points (Fig. 5g, left). Exposure to linear GBCA resulted in an intensively stained, immensely diffuse cytosolic pattern at 4 h, with a similar yet reduced response at 24 h (Fig. 5g, middle). A 4-h macrocyclic GBCA exposure resulted in a brightly diffuse staining pattern compared to untreated controls; following 24-h exposure, CTSD staining displayed reduced diffusion but limited co-staining with LAMP-1 (Fig. 5g, right). Smaller cleaved CTSD (~27 kDa) is released first from the lysosome, followed by the larger CTSB (~37 kDa) (Wang et al. 2018a, b), indicating size exclusivity of released lysosomal content. The differences in immunofluorescent staining patterns of CTSB and CTSD in this exposure model suggest that GBCAs induce partial lysosomal membrane permeabilization. These findings indicate that GBCA-induced pLMP is a dynamic process.

Linear GBCA-induced pLMP impacts mitochondrial function and cell viability

Cell homeostasis depends upon properly functioning organelles working in concert to adapt to changes in the cellular environment (Petkovic et al. 2021). Given that in vivo data demonstrates that not only are endolysosomes impacted by GBCA exposures but mitochondria as well (Supplementary Fig. S1) (DeAguero et al. 2023), it was essential to understand whether the organelle injury occurred in parallel or was interconnected. We also monitored mitochondrial dynamics and network morphology in response to GBCA exposures to explore this potential relationship. Renal tubular cells are rich in mitochondria, with a filamentous, interconnected network that facilitates essential transport functions (Zhan et al. 2013). To evaluate the impact of GBCA exposure on the mitochondrial network of MRPTEpiCs, we utilized live-cell confocal imaging of MitoTracker Red-FM-stained cells to quantitate changes in mitochondrial structure. A 4 h exposure to either the linear or macrocyclic contrast agent resulted in no changes to the characteristic filamentous mitochondrial morphology as mitochondria's mean area, mean perimeter, and aspect ratio are maintained across untreated and treatment groups (Supplementary Fig. S5a-b). Mitochondrial membrane potential was also measured using fluorescent tetramethylrhodamine ethyl ester (TMRE) dye as it is a direct indicator of mitochondrial health owing to the capacity of positively charged dye to accumulate in the mitochondrial matrix dependent upon mitochondrial membrane potential ($\Delta\psi M$). When MRPTEpiCs are exposed to either GBCA for 4 h, the TMRE relative fluorescence is consistent across all groups, indicating intact mitochondrial membrane potential (Supplementary Fig. S5c). The data suggests that 4-h GBCA exposure does not directly impact mitochondrial health.

Given that we see a lysosomal-mediated response as early as 4 h GBCA exposure and that the mitochondria are intact and functional at that time point, we speculated that pLMP occurs upstream of cell injury and that the release of lysosomal proteases plays a role in the loss of cell viability at 24 h (see Fig. 2). To examine the impact of GBCAs and lysosomal proteases on mitochondrial health and cell viability, we studied the effect of GBCAs in tandem with a broad specificity lysosomal protease inhibitor cocktail (PI) and the selective cathepsin B inhibitor CA-074Me for the 24 h exposure period. Parameters of the mitochondrial network were quantified in live-cell images. There is a visible structural shortening of the mitochondria in response to either linear or

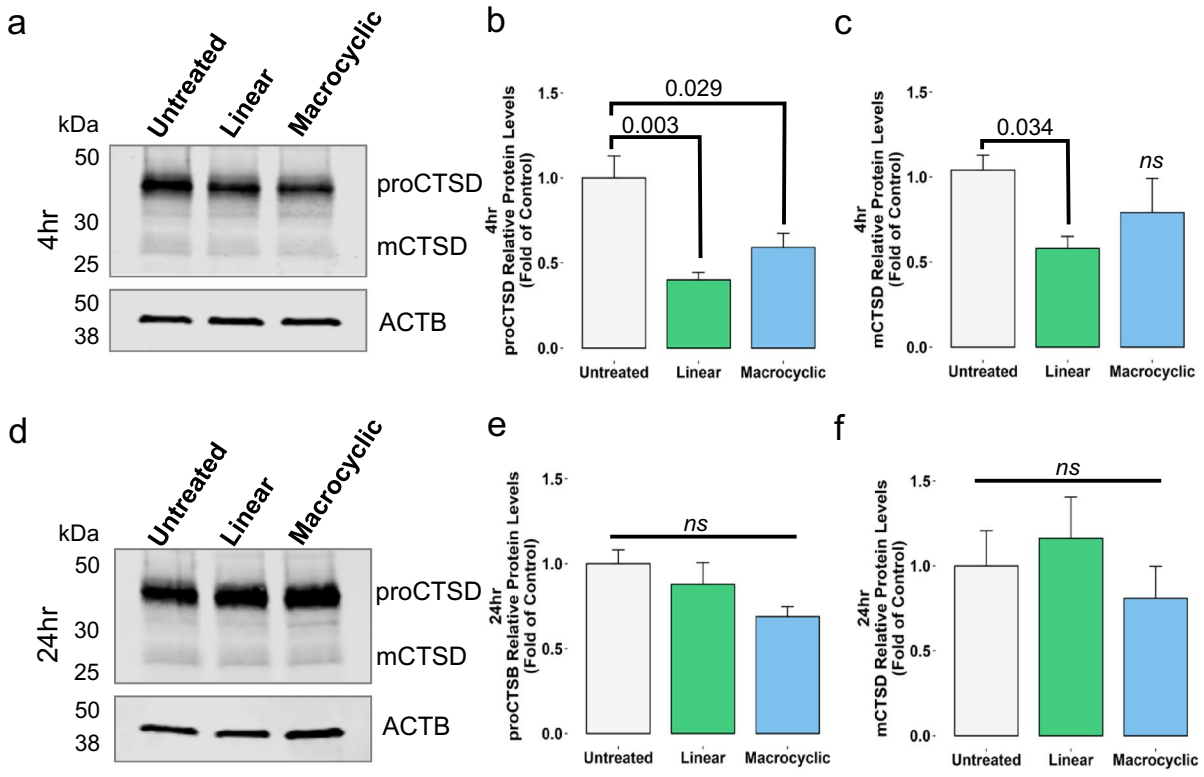

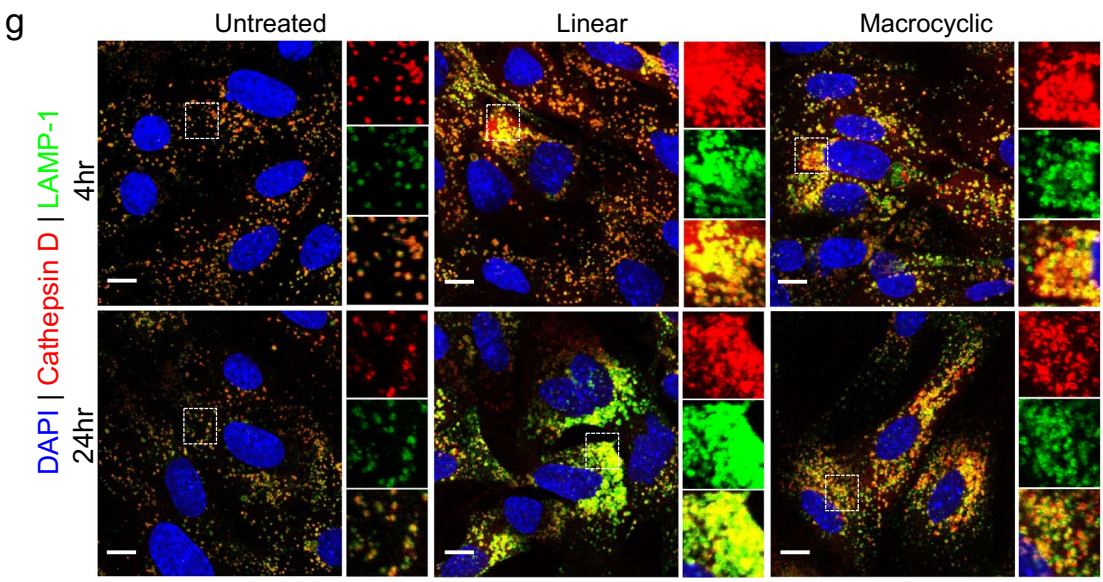

macrocyclic GBCA exposure at 24 h, while linear displayed increased shortening (Fig. 6a). Co-incubation of the GBCAs with PI or CA-074Me blocked this effect. Quantifying mitochondrial morphological parameters highlights that 24 h exposure to linear GBCA significantly reduces the mean area, mean perimeter, and aspect ratio of mitochondria, indicating increased mitochondrial fragmentation (Fig. 6b).

◂**Fig. 5** Impact of GBCA exposure on cathepsin D processing and release from lysosomal lumen. **a**. Western blot showing levels of CTSD in 4 h exposed MRPTEpiCs. **b-c**. Quantification of relative proCTSD and mCTSD levels in untreated and exposed groups. **d**. Representative western blot displaying expression levels of CTSD following 24 h GBCA exposures. **e–f**. Quantitative analysis of relative protein levels of proCTSD and mCTSD after exposure. **b-c-e–f**. Results are represented as mean ± SEM ($n = 4$ per group). The *p*-values are denoted numerically, *ns* = not significant, by One-way ANOVA, Tukey honesty significant difference post-hoc testing. **g**. Confocal images of GBCA-exposed MRPTEpiCs highlighting CTSD staining patterns relative to LAMP-1 staining from at least three independent experiments. Inset dashed boxes indicate regions of interest emphasized by magnified adjacent images: CTSD (Upper), LAMP-1 (Middle), and Merge (Lower). Nuclei were counterstained with DAPI. Leica TCS SP8. Bars = 10 µm

PI and CA-07Me co-treatment with linear GBCA blocked this fragmentation. In contrast, PI co-treatment preserved mitochondrial mean area to a greater degree. Macrocyclic GBCA exposure resulted in a significant decrease in mitochondrial mean area. In contrast, the mean perimeter and aspect ratio were non-significantly changed, demonstrating a shortening of the mitochondrial network rather than its fragmentation (Fig. 6b). Either PI or CA-07Me co-treatment blocked this macrocyclic-induced shortening effect to that of untreated controls.

Next, we investigated if these structural changes to the mitochondrial network impacted mitochondrial activity. Only 24 h linear GBCA exposure resulted in decreased TMRE relative fluorescence, indicating a collapse of the mitochondrial membrane potential (Fig. 6c). This reduction in mitochondrial membrane potential was rescued in the presence of either lysosomal protease inhibitor, indicating that linear GBCA-induced pLMP impacted mitochondrial function. Macrocyclic GBCA exposure, with or without lysosomal protease inhibitors, displayed no impact on mitochondrial membrane potential. As we found that 24-h linear GBCA exposure resulted in reduced metabolic capacity of the treated cells, we monitored cell viability in the GBCA and lysosomal protease inhibitor groups. Both PI and CA-074Me co-incubation with linear GBCA salvaged the metabolic capacity of the exposed cells, while CA-07Me returned viability near that of untreated controls (Fig. 6d). Macrocyclic GBCA and co-incubation with PI had no impact on viability. However, co-incubation of the macrocyclic agent with CA-07Me drastically increased cell viability. Altogether, the lysosomal damage caused by GBCA exposures, primarily linear GBCA, induced functional damage to the mitochondrial network and impacted overall MRPTEpiC health, which appears to be cathepsin dependent.

Discussion

Multiple cell types have been subject to Gd^{3+} or GBCA exposures. Oxidative stress, autophagy, inflammation, and apoptosis have been implicated in the pathogenesis of GBCA or Gd^{3+} toxicity (Coimbra et al. 2024). Several studies have put mitochondrial dysfunction in the foreground as a critical contributor to these toxic outcomes, but the organelle may not be contributing alone (Bower et al. 2019). Short incubation periods with GBCAs alter lysosomal morphology, but the exact mode of action is unknown (Do et al. 2019). Herein, the work provides the first insight into how GBCAs compromise lysosomal function, induce partial permeabilization of the lysosomal membrane, and how this damage modulates mitochondrial function.

For these studies, we investigated how two commercially available GBCAs with differing structural subtypes, stabilities, and charges (Table 1) impacted the endolysosomal system of renal proximal tubule epithelial cells. In the clinical setting, intravenously injected GBCAs will be distributed in the blood and extracellular space, where they will be primarily eliminated intact by the kidneys (Wahsner et al. 2019). Renal proximal tubules not only play an active role in the excretion of xenobiotics and other endogenous compounds, but proximal epithelial cells are often the site of early tubule injury and contribute significantly to the pathogenesis of kidney disease and nephrotoxicity (Yin and Wang 2016). In companion to our previous in vivo linear GBCA study (DeAguero et al. 2023), we found that repeated exposure to macrocyclic GBCAs in the setting of normal renal function resulted in a similar phenotype (Supplementary Fig. S1). The morphological changes to macrocyclic GBCA-exposed renal epithelia were less radical when compared to linear exposed animals, but a pattern of cellular injury was beginning to emerge. Similar insults were identified: dysmorphic mitochondria, enlarged endosomes with abnormal cargo, and lipid accumulation (Supplementary Fig. S1a). In addition to the cellular hoarding of lipids, both

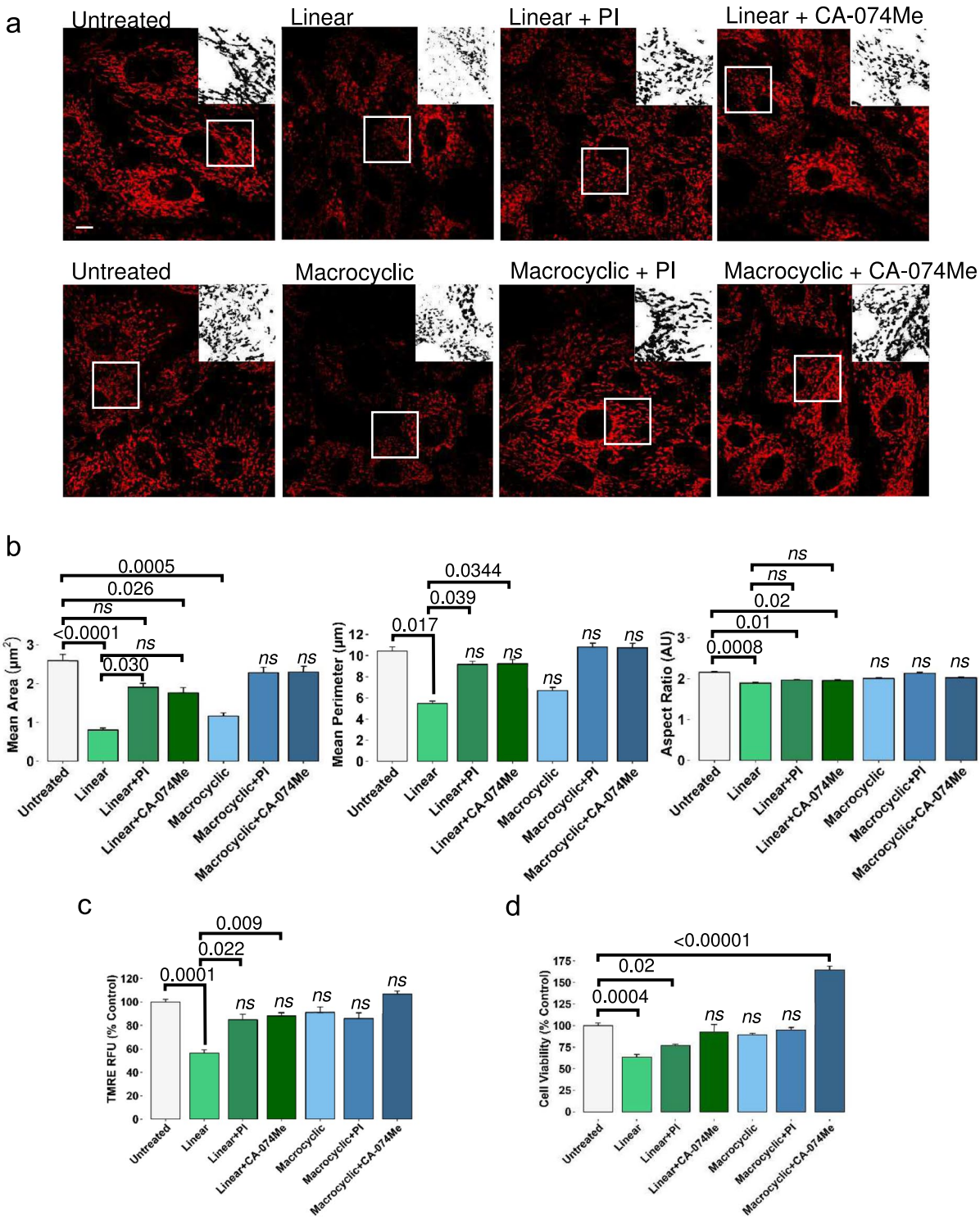

groups (linear and macrocyclic) developed intracellular concentric structures, often referred to as lamellar bodies (Supplementary Fig. S1b). This, in addition to the other pathological changes, pointed to possible GBCA-induced phospholipidosis and the involvement of the lysosome (Anderson and Borlak

◂**Fig. 6** Effect of lysosomal protease inhibition on the mitochondria structure and function in GBCA-treated MRPTEpiCs. **a**. Representative confocal images of labeled mitochondria following 24 h GBCA exposure plus co-treatment with the indicated lysosomal protease inhibitors. Live cells loaded with 250 nM MitoTracker Red-FM. Leica TCS SP8. Bars = 10 µm. Insets are processed, binary images produced in FIJI/Image J. **b**. Mitochondrial network analysis of MitoTracker Red live probed cells using the FIJI/ImageJ Mitochondria Analyzer plugin. Distribution of the mean mitochondrial area and mean mitochondrial perimeter in treated cells. Mitochondrial aspect ratio (length/width) was calculated using the plugin. Results are represented as mean ± SEM from ≥ 75 cells ($n = 3$). The *p*-values are denoted numerically, *ns* = not significant, denoted by line in the graph, or from Untreated, by One-way ANOVA, Tukey honesty significant difference post-hoc testing. **c**. Quantitative analysis of mitochondrial membrane potential ($\Delta\Psi m$) using tetramethylrhodamine ethyl ester (TMRE). Results of relative fluorescence are represented as mean ± SEM ($n = 3$). *ns* = not significant from Untreated, by One-way ANOVA, Tukey honesty significant difference post-hoc testing. **d**. Effect of lysosomal protease inhibitor co-treatment with GBCAs on the metabolic capacity of exposed cells as a measure of cell viability. Data are represented as mean ± SEM ($n = 3$ per group). The *p*-values are denoted numerically, *ns* = not significant from Untreated, by One-way ANOVA, Tukey honesty significant difference post-hoc testing. Protease inhibitor cocktail (PI) (P1860, Sigma-Aldrich). CA-074 methyl ester (CA-074Me) (S7420, SelleckChem)

2006). We then postulated that the lysosome played a more prominent role in the pathogeny of GBCA-induced injury than initially believed. Given this, we exposed mouse renal proximal tubule epithelial cells to either linear or macrocyclic GBCAs (Fig. 1a) using a physiologic concentration of 2 mM (Friebe et al. 2018). The 2 mM concentration is near-physiological blood concentration, which can be calculated from the administered dose of GBCA (0.1 mmol/kg) and estimated blood volume per body weight (60–80 mL/kg). It is a routine concentration used in our previous in vitro studies (Do et al. 2014). The goal of using such a concentration is to mimic those following clinical administrations of GBCAs. Given that the kidney, including renal proximal tubule epithelial cells, plays a primary role in GBCA elimination, it can be justified that these cells will be exposed to these agents for many hours. In states of normal renal function, the kidneys will eliminate > 90% of the intact agent; this elimination period is extended in states of kidney disease (Wahsner et al. 2019). This puts patients at a greater risk for gadolinium-induced complications. In addition, the kidney, primarily the renal cortex, has a consistent history of being one of the tissues with the highest gadolinium concentrations across the board (Do et al. 2019; Le Fur et al. 2023). The present study addressed the influence of short- and longer-term incubation periods of GBCAs at a near-physiological concentration in an in vitro setting.

The cellular uptake of GBCAs has yet to be fully investigated. Using ICP-MS bulk analysis of MRPT-EpiCs exposed to either linear or macrocyclic, we were able to demonstrate that these cells will accumulate gadolinium in a time-dependent manner (Fig. 1b). The intracellular accumulation of gadolinium indicates a GBCA uptake process, which is crucial in understanding the mechanisms of cellular injury. Utilizing an XTT assay to measure cell viability as a function of metabolic capacity, we found that cells showed a contrast agent and time-dependent response. Cells only exposed to linear GBCAs for 24 h displayed a significant loss in cell viability, as no differences were noted in the other time and macrocyclic groups (Fig. 2a). As 24 h linear GBCA exposure resulted in the suppression of cell viability, we also monitored the expression of kidney injury molecule-1 (KIM-1). Upon insult, this specific kidney injury biomarker will be upregulated in the proximal tubule (Song et al. 2019). We found that 24 h linear GBCA exposure drastically increased KIM-1 expression (Fig. 2b), indicating GBCA-induced cell injury. Even though there appears to be an agent and time specificity for detecting cell injury, we cannot discredit what is occurring upstream of these endpoints.

Data thus far indicate that linear GBCAs impact the tested cellular outcomes, but it was important for this study to determine if lysosomes play a role in this pathway. Once believed to be an auxiliary organelle, lysosomes have proven indispensable for cellular homeostasis as they govern multiple signaling pathways, contribute to autophagy, and mediate specific cell death scenarios (Patra et al. 2023). LysoTracker Red staining of GBCA-exposed cells revealed time-dependent changes in lysosomal integrity, as there was a loss of ability for the dye to accumulate in acidic compartments, namely late endosomes, and lysosomes, at 4 h exposure (Fig. 2c-d). In addition, the drastic increase of LTR fluorescence at 24 h is contributed to an increase in LTR-positive puncta populations (Supplementary Fig. S2), indicating a GBCA-mediated lysosomal biogenesis. Lysosomotropic compounds have been reported to result in a similar LTR response (Lu et al. 2017). More specifically,

lysosomotropic compounds that induce some degree of lysosomal stress have been demonstrated to activate the autophagy-lysosome biogenic response to restore the cell to homeostatic conditions (Jeong et al. 2021). So far, the results imply that GBCAs, regardless of class, exhibit lysosomotropic behaviors and induce lysosomal stress shortly into the exposure period.

Like other critical organelles, lysosomes are not static but highly responsive to numerous cellular cues. Alterations to lysosomal size indicate how cells adapt to meet the degradative or metabolic needs of the cell and its functionality (Bussi and Gutierrez 2024). Non-surprisingly, changes in endosome or lysosome (endolysosome) size can significantly influence the dynamics of intracellular trafficking (Bandyopadhyay et al. 2014). Lysosomal size is altered in certain disease states, primarily in lysosomal storage disorders (LSD), where the characteristically enlarged organelle is causally linked to genetic alterations that perturb the synthesis and/or trafficking of lysosomal proteins or cargo (Mächtel et al. 2023). Interestingly, lysosomotropic compounds elicit a similar response in that lysosomal distribution and size are greatly influenced by the lysosomal sequestration of the compound and will often pathologically mimic LSD (Kuzu et al. 2017). Whether in LSD or the sequestration of lysosomotropic compounds, the accumulation of nondegradable material within lysosomes will profoundly impact the organelle's dynamics and function. We demonstrated that a 4 h GBCA exposure induced early lysosomal enlargement in both GBCA groups, as denoted by an increase in LAMP-1 organelle diameter (Fig. 3). This enlargement coincided with galectin-3 redistribution, indicating GBCA-induced lysosomal injury. A 24 h GBCA exposure period resulted in continual endolysosomal enlargement, highlighting the risk for lysosomal dysfunction. As mentioned, lysosome size can substantially influence lysosomal function. Treatment with the lysosomotropic compound chloroquine leads to lysosomal expansion and causes these lysosomes to lose access to the endocytic pathway (Cardoso et al. 2023). This suggests that lysosomotropism of compounds plays a part in inhibiting the transport of essential lysosomal components to the lysosome for proper function. Normal lysosomal processes, including protein degradation or clearance of damaged organelles, depend not only on an optimal acidic pH but also on the presence of functional enzymes necessary for proteolytic degradation and other cellular functions (Hu et al. 2015). Cathepsins, a principal class of lysosomal proteases, depend not only on proper endocytic sorting of pro-cathepsins into endolysosomes but also on the proteolytic activation of mature forms in the acidic environment of the late endosome or lysosome. This prompted us to monitor the processing of two major cathepsins, cysteine protease cathepsin B and aspartic protease cathepsin D (Yadati et al. 2020). As seen in Fig. 4a-c, linear and macrocyclic GBCA exposure at 4 h interfered with the maturation of CSTB. In addition, a 4 h exposure to either agent resulted in decreased levels of proCTSD, indicating reduced transport of the pro-cathepsin (Fig. 5a-b). Interestingly, linear GBCA exposure obstructed CTSD maturation. The final maturation step of CTSD is dependent upon the proteolytic activity of CTSB, in addition to cathepsin L (Mijanovic et al. 2021). Our data indicates that early GBCA exposure results in a loss of lysosomal function by not only impacting the transport of pro-cathepsins into the endolysosomal system but also creating a hostile lysosomal environment.

Even though the expression of both forms of CTSB and CTSD were returned to near untreated levels following 24 h GBCA exposure, earlier data, including the increase in lysosomal populations (Supplementary Fig. S2) and continued enlargement (Fig. 3), suggest persistent and widespread lysosomal dysfunction. Interestingly, CTSB activity is increased following 24 h GBCA exposure (Supplementary Fig. S4b), which may play an exacerbating role in lysosomal dysfunction or represent a damage response mechanism, warranting future studies. Thus far, we have highlighted several factors that influence lysosomal enlargement. The activity of enlarged lysosomes is often impaired, resulting in the accumulation of undegraded material, as seen in LSD. Failure of cathepsin processing is partly a consequence of lysosomal enlargement and vice versa (Jung et al. 2015). Lysosomotropic agents have demonstrated the ability to induce lysosomal enlargement and lysosomal membrane permeabilization (Villamil Giraldo et al. 2014). LMP is an exceedingly dynamic process that involves the destabilization of the lysosomal membrane and the liberation of lysosomal content into the cytoplasm, including cathepsins, which activate compensatory mechanisms to restore cell function or initiate a cell death cascade (Wang et al. 2018a, b). Next, we attempted to determine if the enlarged lysosomes in

GBCA-exposed cells were prone to LMP. Data thus far have suggested the possibility of GBCA-induced LMP, including the loss of LTR fluorescence at 4 h exposure (Fig. 2c-d) and the galectin-3 puncta assay (Fig. 3c). A distinctive feature of LMP is the release of lysosomal content to the cytosol, which can be determined by monitoring the translocation of cathepsins from the lysosomal lumen to the cytosol (Aits et al. 2015a, b). Given this, the lysosomal enlargement seen as early as 4 h exposure coincides with the translocation of CTSB and CTSD to the cytosol (Figs. 4g and 5g, respectively), supporting GBCA-induced LMP. The staining patterns, however, indicate that this is not a complete destabilization of the lysosomal membrane, as CTSD is far more diffuse and widespread than CTSB staining. Data also indicate a more significant response is elicited in the linear GBCA-exposed groups. This suggests that the smaller CTSD is released more easily than the larger CTSB, indicating partial lysosomal membrane permeabilization (Wang et al. 2018a, b). Leakage of lysosomal contents, including proteases, into the cytosol can trigger cell death modalities. These can include lysosome-dependent cell death or cathepsin-mediated activation of apoptotic substrates, including Bid and Bax, leading to permeabilization of the mitochondrial outer membrane and induction of apoptosis (Serrano-Puebla and Boya 2016).

Since endolysosomes will physiochemically interact with other organelles, including, but not limited to, mitochondria, it suggests that inter-organelle signaling may affect organellar stress responses (Lakpa et al. 2021). Lysosomal membrane damage and the release of lysosomal proteases have been shown to directly impact mitochondrial function by triggering the degradation of mitochondrial proteins, resulting in altered cell metabolism (Bussi et al. 2022). Given this, we also monitored the integrity of the mitochondrial network at our treatment time points. There was no indication of mitochondrial dysfunction following 4 h GBCA exposure (Supplementary Fig. S5), indicating that GBCA-induced pLMP occurs upstream of cell stress. To further validate that the selective release of CTSD and CTSB is actively involved in the loss of metabolic function seen in the 24 h linear GBCA group (Fig. 2a), we co-treated MRPTEpiCs with a broad specificity lysosomal protease inhibitor, which contains E64 (cysteine protease inhibitor), Leupeptin (serine and cysteine protease inhibitor) and Pepstatin A (aspartic protease inhibitor) or CTSB specific inhibitor CA-074Me. In this exposure model, we demonstrated that both classes of GBCAs induce a structural shortening of the mitochondria. Still, linear GBCA exposure alone resulted in profound mitochondrial fragmentation and loss of mitochondrial activity. This linear GBCA-induced effect was ameliorated in both protease inhibitor groups, as mitochondrial network morphology and mitochondrial membrane potential were restored to near untreated levels (Fig. 6). Furthermore, the metabolic capacity of linear GBCA-exposed cells co-treated with lysosomal protease inhibitors was rescued, indicating that released CTSB and CTSD play a primary role in mitochondrial dysfunction.

This study has some limitations. We used a 2D in vitro model of mouse renal proximal tubule epithelial cells to explore the direct nephrotoxic effect of GBCAs. One must be conscientious when translating these results, as they may not directly reflect the clinical setting. In this study, we instead provide a foundation for future studies with human renal proximal tubular epithelial cells. We addressed the release of cathepsins and their role in GBCA-induced injury. Still, the effect of other lysosomal contents, including calcium (Ca^{2+}), iron (Fe^{2+}), or lysosomal-derived reactive oxygen species (ROS), could provide further insight into the detailed mechanism of GBCA-induced nephrotoxicity. Additionally, this work will allow us to expand into other organelle-specific pathways of injury and cell death, as the profound vacuolization and fragmented nuclei seen in Fig. 3e indicate that cell death pathways may be initiated because of GBCA exposure.

Organelle autonomy is outdated. Under stressful cellular conditions, organelles will autoregulate and initiate stress responses to meet the needs of the cell and return it to homeostatic conditions (Sasaki and Yoshida 2015). In the transition from acute kidney injury to chronic kidney disease, mitochondrial-endoplasmic reticulum stress and crosstalk are well-studied and highly attributed to disease progression (Maekawa and Inagi 2019). In comparison, the need to understand the lysosomal stress response and the potential for crosstalk with other organelles is rising. Our data indicates that linear and macrocyclic GBCAs are taken up intracellularly, at similar concentrations, and impart similar effects in mouse renal proximal tubule cells, but linear GBCA exposure

induces a more significant toxic outcome. This may be attributed to the ease and quantity with which the non-ionic linear GBCA is trafficked into the endolysosomal system, compared to the negatively charged macrocyclic GBCA, as the physicochemical properties of the agent can influence GBCA uptake (Gianolio et al. 2011). Future work will address this possibility. A possible mechanism of GBCA-induced nephrotoxicity in renal proximal tubule epithelial cells is identified (Fig. 7). First, lysosomal sequestration of GBCAs induces lysosomal enlargement and failure of cathepsin processing results, leading to lysosomal dysfunction. Second, GBCA-induced lysosomal enlargement results in partial lysosomal membrane permeabilization and the release of cathepsins, which modulate mitochondrial activity and cell function. Our data provide insight into how GBCA-induced damage impacts mitochondrial function and identifies potential therapeutic targets to alleviate the toxic effects of GBCAs.

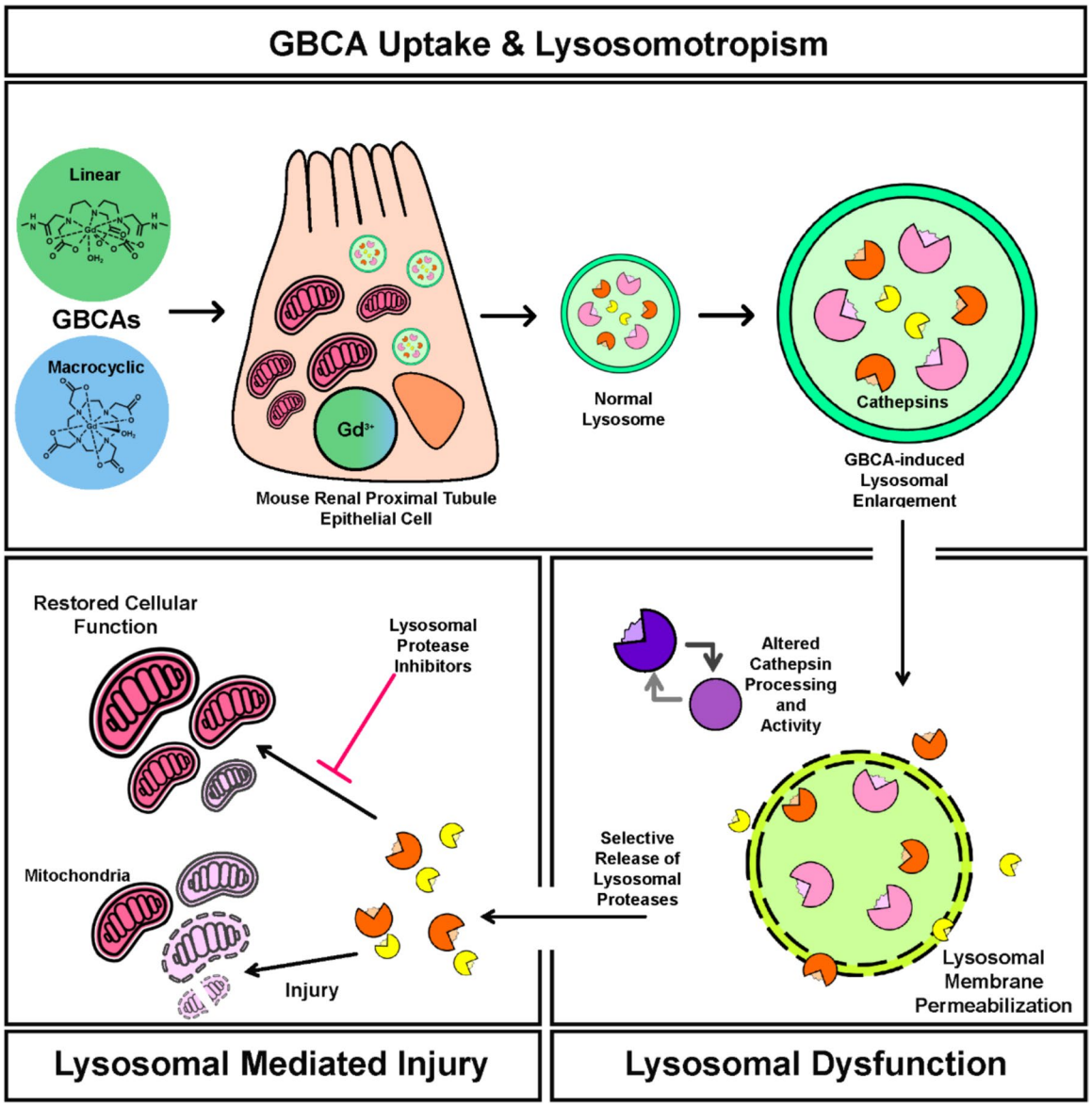

Fig. 7 GBCA-induced mechanism of lysosomal mediated mouse renal proximal tubule epithelial cell injury

Acknowledgements BW is an associate member of the Autophagy, Inflammation, and Metabolomics (AIM) Center of Biomedical Research Excellence (NIH grant P20GM121176). Data were generated in the HSC-Electron Microscopy Facility, supported by The University of New Mexico Health Sciences Center. Inductively coupled plasma mass spectrometry analysis was performed by the Analytical Geochemistry Laboratory in the University of New Mexico Department of Earth & Planetary Sciences. Support for in vivo experiments in this paper was provided by the University of New Mexico Cancer Center Animal Models Shared Resource, funded by NCI 2P30 CA118100 (PI Willman, C.) "UNM Cancer Center Support Grant". This research was partially supported by UNM Comprehensive Cancer Center Support Grant NCI P30CA118100 and made use of the Fluorescence Microscopy and Cell Imaging shared resource. This research was partially supported by UNM Comprehensive Cancer Center Support Grant NCI P30CA118100 and the Flow Cytometry shared resource.

Author contributions Conceptualization of study design was by J.D. and B.W.. Experimental procedures conducted by J.D.. Electron microscopy preparation and imaging was performed by J.D. and T.H.. Statistical analysis was performed by J.D. and B.W.. J.D. wrote the main manuscript text and prepared all figures. All authors reviewed and edited the manuscript.

Funding The research was funded by a Veterans Administration Merit Award (I01 BX001958, BW), a National Institutes of Health R01 grant (DK-102085), and Dialysis Clinic, Inc. This project was supported in part by the Dedicated Health Research Funds of the University of New Mexico School of Medicine allocated to the Signature Program in Cardiovascular and Metabolic Disease (CVMD), National Center for Research Resources and the National Center for Advancing Translational Sciences of the National Institutes of Health through Grant Number UL1TR001449 (CTSC/DCI Kidney Pilot Project CTSC004-12 and CTSC/Environmental Health Signature Program Pilot Project CTSC003-13) and partial support by the University of New Mexico (UNM) Brain and Behavioral Health Institute (BBHI 2018–1008, 2020–21-002), and UNM School of Medicine Research Allocation Committee (C-2459-RAC, New Mexico Medical Trust). JD is supported by the National Center for Advancing Translational Sciences, National Institutes of Health Diversity Supplement (3UL1TR001449-08S1).

Data availability No datasets were generated or analysed during the current study.

Declarations

Ethical approval All animal protocols for experiments were approved by the University of New Mexico's Institutional Animal Care and Use Committee (IACUC) under protocol 21–201088-HSC, Animal Welfare Assurance #D16-00228, A3350-01, USDA Registration #85-R-0014.

Competing interests The authors declare no competing interests.

References

Aits S, Jäättelä M, Nylandsted J. Methods for the quantification of lysosomal membrane permeabilization: a hallmark of lysosomal cell death. Methods Cell Biol. 2015a;126:261–85.

Aits S, Kricker J, Liu B, Ellegaard AM, Hämälistö S, Tvingsholm S, Corcelle-Termeau E, Høgh S, Farkas T, Holm Jonassen A, Gromova I, Mortensen M, Jäättelä M. Sensitive detection of lysosomal membrane permeabilization by lysosomal galectin puncta assay. Autophagy. 2015b;11(8):1408–24.

Anderson N, Borlak J. Drug-induced phospholipidosis. FEBS Lett. 2006;580(23):5533–40.

Bandyopadhyay D, Cyphersmith A, Zapata JA, Kim YJ, Payne CK. Lysosome transport as a function of lysosome diameter. PLoS One. 2014;9(1):e86847.

Bower DV, Richter JK, von Tengg-Kobligk H, Heverhagen JT, Runge VM. Gadolinium-based MRI contrast agents induce mitochondrial toxicity and cell death in human neurons, and toxicity increases with reduced kinetic stability of the agent. Invest Radiol. 2019;54(8):453–63.

Bussi C, Gutierrez MG. One size does not fit all: Lysosomes exist in biochemically and functionally distinct states. PLoS Biol. 2024;22(3):e3002576.

Bussi C, Heunis T, Pellegrino E, Bernard EM, Bah N, Dos Santos MS, Santucci P, Aylan B, Rodgers A, Fearns A, Mitschke J, Moore C, MacRae JI, Greco M, Reinheckel T, Trost M, Gutierrez MG. Lysosomal damage drives mitochondrial proteome remodelling and reprograms macrophage immunometabolism. Nat Commun. 2022;13(1):7338.

Cao M, Luo X, Wu K, He X. Targeting lysosomes in human disease: from basic research to clinical applications. Signal Transduct Target Ther. 2021;6(1):379.

Cardoso MH, Hall MJ, Burgoyne T, Fale P, Storm T, Escrevente C, Antas P, Seabra MC, Futter CE. Impaired lysosome reformation in chloroquine-treated retinal pigment epithelial cells. Invest Ophthalmol vis Sci. 2023;64(11):10.

Chaudhry A, Shi R, Luciani DS. A pipeline for multidimensional confocal analysis of mitochondrial morphology, function, and dynamics in pancreatic β-cells. Am J Physiol Endocrinol Metab. 2020;318(2):E87-e101.

Coimbra S, Rocha S, Sousa NR, Catarino C, Belo L, Bronzeda-Rocha E, Valente MJ, Santos-Silva A. Toxicity mechanisms of gadolinium and gadolinium-based contrast agents-a review. Int J Mol Sci. 2024;25(7):4071.

Davies J, Siebenhandl-Wolff P, Tranquart F, Jones P, Evans P. Gadolinium: pharmacokinetics and toxicity in humans and laboratory animals following contrast agent administration. Arch Toxicol. 2022;96(2):403–29.

DeAguero J, Howard T, Kusewitt D, Brearley A, Ali AM, Degnan JH, Jett S, Watt J, Escobar GP, Dokladny K, Wagner B. The onset of rare earth metallosis begins with renal gadolinium-rich nanoparticles from magnetic resonance imaging contrast agent exposure. Sci Rep. 2023;13(1):2025.

Do C, Barnes JL, Tan C, Wagner B. Type of MRI contrast, tissue gadolinium, and fibrosis. Am J Physiol Renal Physiol. 2014;307(7):F844-855.

Do C, Ford B, Lee DY, Tan C, Escobar P, Wagner B. Gadolinium-based contrast agents: stimulators of myeloid-induced renal fibrosis and major metabolic disruptors. Toxicol Appl Pharmacol. 2019;375:32–45.

Do QN, Lenkinski RE, Tircso G, Kovacs Z. How the chemical properties of GBCAs influence their safety profiles in vivo. Molecules. 2021;27(1):58.

Friebe B, Godenschweger F, Fatahi M, Speck O, Roggenbuck D, Reinhold D, Reddig A. The potential toxic impact of different gadolinium-based contrast agents combined with 7-T MRI on isolated human lymphocytes. Eur Radiol Exp. 2018;2(1):40.

Gianolio E, Arena F, Strijkers GJ, Nicolay K, Högset A, Aime S. Photochemical activation of endosomal escape of MRI-Gd-agents in tumor cells. Magn Reson Med. 2011;65(1):212–9.

Heinrich MC, Kuhlmann MK, Kohlbacher S, Scheer M, Grgic A, Heckmann MB, Uder M. Cytotoxicity of iodinated and gadolinium-based contrast agents in renal tubular cells at angiographic concentrations: in vitro study. Radiology. 2007;242(2):425–34.

Hermann P, Kotek J, Kubícek V, Lukes I. Gadolinium(III) complexes as MRI contrast agents: ligand design and properties of the complexes. Dalton Trans. 2008;(23):3027–47.

Hu YB, Dammer EB, Ren RJ, Wang G. The endosomal-lysosomal system: from acidification and cargo sorting to neurodegeneration. Transl Neurodegener. 2015;4:18.

Jeong SJ, Stitham J, Evans TD, Zhang X, Rodriguez-Velez A, Yeh YS, Tao J, Takabatake K, Epelman S, Lodhi IJ, Schilling JD, DeBosch BJ, Diwan A, Razani B. Trehalose causes low-grade lysosomal stress to activate TFEB and the autophagy-lysosome biogenesis response. Autophagy. 2021;17(11):3740–52.

Jung M, Lee J, Seo HY, Lim JS, Kim EK. Cathepsin inhibition-induced lysosomal dysfunction enhances pancreatic beta-cell apoptosis in high glucose. PLoS One. 2015;10(1):e0116972.

Kuzu OF, Toprak M, Noory MA, Robertson GP. Effect of lysosomotropic molecules on cellular homeostasis. Pharmacol Res. 2017;117:177–84.

Lakpa KL, Khan N, Afghah Z, Chen X, Geiger JD. Lysosomal stress response (LSR): physiological importance and pathological relevance. J Neuroimmune Pharmacol. 2021;16(2):219–37.

Lawrence RE, Zoncu R. The lysosome as a cellular centre for signalling, metabolism and quality control. Nat Cell Biol. 2019;21(2):133–42.

Le Fur M, Moon BF, Zhou IY, Zygmont S, Boice A, Rotile NJ, Ay I, Pantazopoulos P, Feldman AS, Rosales IA, How I, Izquierdo-Garcia D, Hariri LP, Astashkin AV, Jackson BP, Caravan P. Gadolinium-based contrast agent biodistribution and speciation in rats. Radiology. 2023;309(1):e230984.

Li Z, Liu Z, Luo M, Li X, Chen H, Gong S, Zhang M, Zhang Y, Liu H, Li X. The pathological role of damaged organelles in renal tubular epithelial cells in the progression of acute kidney injury. Cell Death Discov. 2022;8(1):239.

Lohrke J, Frenzel T, Endrikat J, Alves FC, Grist TM, Law M, Lee JM, Leiner T, Li KC, Nikolaou K, Prince MR, Schild HH, Weinreb JC, Yoshikawa K, Pietsch H. 25 years of contrast-enhanced MRI: developments, current challenges and future perspectives. Adv Ther. 2016;33(1):1–28.

Lu S, Sung T, Lin N, Abraham RT, Jessen BA. Lysosomal adaptation: How cells respond to lysosomotropic compounds. PLoS One. 2017;12(3):e0173771.

Mächtel R, Boros FA, Dobert JP, Arnold P, Zunke F. From lysosomal storage disorders to Parkinson's disease - challenges and opportunities. J Mol Biol. 2023;435(12):167932.

Maekawa H, Inagi R. Pathophysiological role of organelle stress/crosstalk in AKI-to-CKD transition. Semin Nephrol. 2019;39(6):581–8.

Mijanovic O, Petushkova AI, Brankovic A, Turk B, Solovieva AB, Nikitkina AI, Bolevich S, Timashev PS, Parodi A, Zamyatnin Jr AA. Cathepsin D-managing the delicate balance. Pharmaceutics. 2021;13(6);837.

Papadopoulos C, Kravic B, Meyer H. Repair or lysophagy: dealing with damaged lysosomes. J Mol Biol. 2020;432(1):231–9.

Patra S, Patil S, Klionsky DJ, Bhutia SK. Lysosome signaling in cell survival and programmed cell death for cellular homeostasis. J Cell Physiol. 2023;238(2):287–305.

Perera RM, Zoncu R. The lysosome as a regulatory hub. Annu Rev Cell Dev Biol. 2016;32:223–53.

Petkovic M, O'Brien CE, Jan YN. Interorganelle communication, aging, and neurodegeneration. Genes Dev. 2021;35(7–8):449–69.

Sasaki K, Yoshida H. Organelle autoregulation-stress responses in the ER, Golgi, mitochondria and lysosome. J Biochem. 2015;157(4):185–95.

Serrano-Puebla A, Boya P. Lysosomal membrane permeabilization in cell death: new evidence and implications for health and disease. Ann N Y Acad Sci. 2016;1371(1):30–44.

Shamam YM, Hashmi MF, De Jesus O. Nephrogenic systemic fibrosis. In: StatPearls [Internet]. Treasure island (FL): StatPearls publishing. 2024.

Sherry AD, Caravan P, Lenkinski RE. Primer on gadolinium chemistry. J Magn Reson Imaging. 2009;30(6):1240–8.

Song J, Yu J, Prayogo GW, Cao W, Wu Y, Jia Z, Zhang A. Understanding kidney injury molecule 1: a novel immune

factor in kidney pathophysiology. Am J Transl Res. 2019;11(3):1219–29.
Turk V, Turk B, Turk D. Lysosomal cysteine proteases: facts and opportunities. Embo J. 2001;20(17):4629–33.
Villamil Giraldo AM, Appelqvist H, Ederth T, Öllinger K. Lysosomotropic agents: impact on lysosomal membrane permeabilization and cell death. Biochem Soc Trans. 2014;42(5):1460–4.
Wahsner J, Gale EM, Rodríguez-Rodríguez A, Caravan P. Chemistry of MRI contrast agents: current challenges and new frontiers. Chem Rev. 2019;119(2):957–1057.
Wang F, Gómez-Sintes R, Boya P. Lysosomal membrane permeabilization and cell death. Traffic. 2018a;19(12):918–31.
Wang F, Salvati A, Boya P. Lysosome-dependent cell death and deregulated autophagy induced by amine-modified polystyrene nanoparticles. Open Biol. 2018b;8(4):170271.
Yadati T, Houben T, Bitorina A, Shiri-Sverdlov R. The ins and outs of cathepsins: physiological function and role in disease management. Cells. 2020;9(7):1679.
Yin J, Wang J. Renal drug transporters and their significance in drug-drug interactions. Acta Pharm Sin B. 2016;6(5):363–73.
Zhan M, Brooks C, Liu F, Sun L, Dong Z. Mitochondrial dynamics: regulatory mechanisms and emerging role in renal pathophysiology. Kidney Int. 2013;83(4):568–81.